ISSN 1027-5495. Functional Materials, 29, No.3 (2022), p. 408-418.
doi:https://doi.org/10.15407/fm29.02.408

Using Brillouin's theorem for obtaining symmetry-preserving and symmetry-breaking solutions. Application to graphene quantum dots

A.V.Luzanov

STC "Institute for Single Crystals", National Academy of Sciences of Ukraine, 60 Lenin Ave., 61001 Kharkiv, Ukraine

Received January 20, 2022

The consistent Brillouin-theorem-based scheme is developed for obtaining numerical Hartree-Fock (HF) solutions at the semiempirical level. Our approach for getting corresponding HF results exploits a general configurational interaction singles procedure for which the compact formulation via only one-electron matrices in AO basis set is applied. The proposed algorithms demonstrate their reliability and feasibility for large-scale conjugated molecules. Particular focus is on finding HF symmetry-preserving and symmetry-breaking solutions of the charge density wave (CDW) type. Among the main systems studied here are graphene quantum dots of periacene type and singlet polyradical structures consisting of triangulene subunits (particularly, π-system of the recently synthesized triangulenic "nanostar") We show that formally incorrect HF solutions of CDW type (occurence of atomic net charges) implicitly reflect a decrease of atomic valencies in highly correlated alternant π-structures.

Keywords: configurational interaction, Hartree-Fock convergence and stability, graphene-like molecules, alternant symmety, π-electrons.

Використання теореми Бриллюена для обчислення розв'язків із збереженою та порушеною симетріями. Застосування до графенових квантових точок. *А.В.Лузанов*

Для отримання чисельних розв'язків рівнянь Гартрі-Фока (HF) в напівемпіричному наближенні розроблено обчислювальну схему, що базується на послідовному використанні теореми Бриллюена. Наш підхід здійснює процедуру самоузгодженого поля за допомогою загальної схеми конфігураційної взаємодії однократних збуджень, щодо якої застосовано компактне формулювання в термінах лише одноелектронних матриць у базисі АО. Запропонований алгоритм демонструє свою надійність та доцільність при застосуванні до великих супряжених молекул. Особливу увагу приділено отриманню HF-розв'язків із збереженою та порушеною симетріям за типом хвилі зарядової густини (CDW). Поміж основних систем, що їх вивчено в роботі, є графенові квантові точки за типом періаценів та синглетні полірадикальні структури, котрі побудовано з триангуленових субодиниць (такі, як нещодавно синтезована триангуленова "нанозіронька"). Ми показуємо, що формально некоректні CDW HF-розв'язки (наявність залишкових атомних зарядів) відзеркалюють зниженння валентностей вуглецевих атомів у сильно коррельованих альтернантних π-структурах.

1. Introduction

Studies of graphene-like molecules and graphene quantum dots (GQDs) are among the active fields of current theoretical, experimental, and material science investigations [1–3]. Many theoretical models of GQDs are based on semiempirical quantum approaches, and here π-electron models are

especially attractive owing to their relative simplicity and feasibility for large-scale conjugated nerworks. Frequently, the starting point in such investigations is obtaining the Hartree- Fock (HF) description (orbital energies, densities of various kind etc.). However, in case of molecular problems, especialy huge ones, researchers may encounter numerical instability and other difficulties in solving nonlinear HF equations. Such issues are often handled in computational chemistry (e.g., see chapter 4 in [4]). Up to now, HF convergency difficulties and their reduction remain one of the topically discussed issues (see, e.g., [5, 6]). The good, solid book [7] also continues to be pertinent for exploring the above mentioned problems.

Among general results of HF and post-HF theories, the Brillouin theorem takes a special place [8–14]. In the present paper this theorem will allow us to propose a simple approach for treating the convergency difficulties in large π-electron problems. We will expose the new algorithm in detail and illustrate it by several large GOD systems as giving an important class of polycyclic aromatic hydrocarbons (PAHs) which allow for nontrivial HF solutions.

2. The Brillouin theorem for HF models

As well known, the Brillouin theorem (BT) states that for self-consistent field (SCF) HF molecular orbitals the Slater one-determinant wave function $|\Phi\rangle$ of the given N-electron state does not interact with any singly excited Slater determinant $\Phi_{i\to a}\rangle$. The latter is built up from $|\Phi\rangle$ by replacing occupied molecular orbital (MO) $|\varphi_i\rangle$ with virtual MO $|\varphi_a\rangle$. Explicitly,

$$\langle\Phi_{i\to a}|H|\Phi\rangle = 0, \qquad (1)$$

where H is the total N-electron Hamiltonian, and in this section all MOs are implied to be MOs with spin, i. e. molecular spin-orbitals. Eq. (1) follows from the variational principle for the HF problem, and it was applied long ago for obtaining HF MOs numerically [8, 12]. The core idea behind it was to use the linear variational function at the singly excited configurational interaction (CIS) level:

$$|\Psi\rangle = c_0|\Phi\rangle + \sum_{i,a}\tau_{ai}|\Phi_{i\to a}\rangle, \qquad (2)$$

where c_0 and τ_{ai} are linear variational paramerers. Indeed, for the given MO set the mixing between $|\Phi\rangle$ and $\Phi_{i\to a}\rangle$ in Eq. (2) is governed by nondiagonal matrix elements f_{ai} of the one-electron Fock operator (Fockian) f for the reference determinant $|\Phi\rangle$. This is a consequence of the common identity for Slater's determinants:

$$\langle\Phi_{i\to a}|H|\Phi\rangle = f_{ai}, \qquad (3)$$

that is valid for any MOs from which superposition (2) is constructed. Thus, the requirement $f_{ai} \equiv 0$ is equivalent to fulfilling BT, Eq. (1), and thence to the standard HF equations.

From the above one can deduce various numerical BT-based algorithms, and the first BT-like scheme was given in the pioneer paper of Lefebvre [8]. Generally, starting from arbitrary (non-self-consistent) full MO set $\{|\varphi_i\rangle\}$, $\{|\varphi_a\rangle\}$ with nonzero f_{ai}, one must approximately solve the CIS problem for c_0 and $\{\tau_{ai}\}$ in Eq. (2), and it allows one to update the starting MOs. Then the computational cycle repeats until Eq. (1) is satisfied within a prescribed accuracy. In practice, solving CIS secular problem for Eq. (2) is replaced by a simplistic estimation of conFigurational coefficients τ_{ai}, and actually the variational potential of Eqs. (1) and (2) is not used fully. At the same time, owing to variational properties of any linear secular problem the total energy must be systematically lowered during the BT-based iterational procedure if all computations are performed carefully and with a proper accuracy. This is a particularly attractive feature of the whole BT approach, and it is this fact that motivates our study which is oriented on computations of large conjugated systems within the semiempirical π-electron framework. The present study is based on the point that CIS problems can be easily implemented if one makes use of suitable CIS matrix formulations from Mestechkin's works [7, 15, 16] and his followers.

3. The BT based matrix algorithm for restricted HF

In this section our BT-SCF matrix scheme is presented for normal ground singlet states within the restricted HF (RHF) method (the unrestricted HF is treated in Appendix). Thus, we start with the general CIS problem (2) for low-lying singlet states. The matrix formulation for the CIS energy

functional was presented first in [17], and then in [15, 16] where the full set of needed relations had been provided in terms of Hermitian transition matrices (with $c_0 = 0$). We follow papers [18, 19] containing similar expressions in a slightly modified form (in terms of ordinary transition matrices). Hereafter we employ matrices in basis of conventional spin-free orbitals (not spin-orbitals as above in Section 2). Recall that within the matrix-covariant methodology all variational parameters are packed, if possible, into pertinent matrices. In case of Eq. (1) the array of conFigurational coefficients $\{\tau_{ai}\}$ turns out to be a one-electron transition matrix τ, as follows:

$$\tau = \|\tau_{ai}\|. \qquad (4)$$

This τ or its Hermitized counterpart $\tau + \tau^+$ can be correctly treated as an operator entity with a prescribed transfomation law for associated matrix elements. It means that one can directly compute τ in the AO basis set as well, and this fact is the leading idea of matrix algorithms for CIS in [16] and books [8, 17]. After these preliminaries, we give our main BT-SCF relations.

As seen from Eq. (2), at each iteration step one must find optimal coefficient c_0 and transition matrix τ for current orbital set $\{\varphi_i\rangle\}$, $\{\varphi_a\rangle\}$. It leads us to solving the uncomplicated eigenvalue problem:

$$\sqrt{2}\mathrm{Tr}f\tau - \lambda c_0 = 0, \qquad (5)$$

$$\hat{\Pi}(\tau) + \sqrt{2}f_{ph}c_0 - \lambda\tau = 0, \qquad (6)$$

where λ is taken as the lowest eigenvalue of the CIS problem to be studied. This gives a guaranteed decrease of the full energy, E^{CIS} , in respect to the RHF energy, E, of the current ground-state Slater determinant $|\Phi\rangle$:

$$E = \mathrm{Tr}(h + f)P, \qquad (7)$$

and hence, the quantity

$$E^{\mathrm{CIS}} = E + \lambda \qquad (8)$$

is the total energy of the general CIS wave function (2). In Eq. (7) h is the usual core Hamiltonian, and P is the key matrix (charge density projector) which projects onto current occupied MO space whereas $I - P$ projects onto virtual MO space; f is the Fockian matrix. Next, Π in Eq. (6) is a superoperator which describes CIS excitations themselves (if $c_0 \equiv 0$) and acts in a space of transition matrices (for precise definition of Π, see Appendix, Eq. (A9)). At last,

$$f_{ph} = (I - P)fP \qquad (9)$$

is the particle-hole component of the Fockian matrix. In MO representation $f_{ph} = \|f_{ai}\|$, and this f_{ph} matrix is in fact a gradient matrix of E in respect to P (more accurately, in respect to independent elements of P). Clearly, when $f_{ph} = 0$, BT in form of Eqs. (1) and (3) is fully satisfied, and thus one arrives at a SCF solution of HF equations. In this limiting case, $\lambda = 0$, so that $E^{\mathrm{CIS}} = E$, that is the final RHF energy.

Given Eqs. (5)–(9), the following BT-SCF procedure can be suggested. Firstly we take the usual Huckel start for P and f: $P_0 \equiv P_{\mathrm{Huck}}$, $f_0 = f[P_0]$, where P_{Huck} is the projector onto Huckel occupied MOs; so that the starting Fockian $f_0 = f[P_0]$ is conventionally computed with this P_0. It gives the initial matrices P_0, f_0 and the initial total energy

$$E_0 = \mathrm{Tr}(h + f_0)P_0. \qquad (10)$$

To proceed further the CIS problem, Eqs. (5) and (6), should be solved more or less pricisely. In our implementation the Lanczos algorithm is employed with a small Krylov space dimension, $\dim K$ (as a rule, $\dim K = 3$ is sufficient). Moreover, a restart of the entire Lanczos process is recommended to be done several (3-5) times. Importantly, all these CIS computations are easily and quickly performed in the π-AO framework (see Appendix for detail). Having at our disposal the current c_0 and τ we easily update the charge density projector, $P \to P_0$, through the known McWeeny equation [20]. In our case it means that

$$P = (P_0 + t)(I + t^+t)^{-1}(P_0 + t^+), \qquad (11)$$

where $t = c_0\tau/\sqrt{2}$.

4. RHF solutions for graphene quantum dots

Now we consiser some applications of the above given BT-based algorithm for RHF solutions in large conjugated systems. For such systems simple gradient-based SCF techniques can be ineffective. Note that as a rule the conventional gradient method with constant step size works well for "normal" π-structures (polyacenes and similar sys-

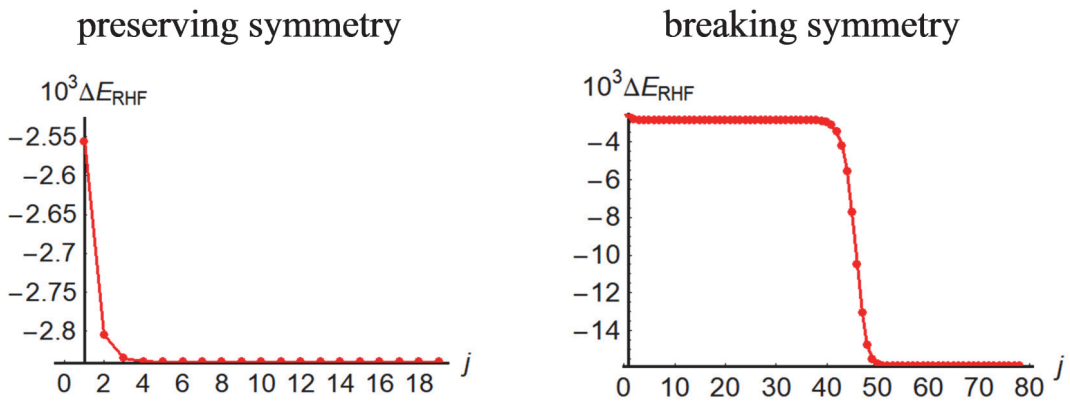

Fig. 1. Electronic energy convergence for the RHF alternant symmetry-preserving and symmetry-breaking (CDW) solutions in (9,6)PA. In abscissa, j is a number of current iteration; ΔE_{RHF} in ordinate is given in au.

tems). Nevertheless, for large π-systems this gradient and similar procedures can lead to numerical instability and even divergence. In the thorough analysis [7] it is shown that the singlet-type HF stability is a necessary condition for convergence of RHF gradient methods (see also [21]). So it is not surprising that it migth be difficult to reach SCF solutions for π-structures of graphene molecules with hundreds carbon atoms since they can suffer from a singlet HF instability (then an additional energy lowering is possible due to admixture of singlet excitations). Recall also that the relevant HF stability analysis, introduced by Cizek and Paldus [22], allows to predict occurrence of symmetry-breaking RHF solutions of certain kinds by detecting negative eigenvalues of HF Hessian (HF stability matrix). For example, symmetry-breaking HF solutions were reported in [23] for long polyenes. On the other hand, special singlet solutions of this type have not been detected even still in long polyacenes if applying usual semiempirical π-parameres.

By and large, singlet HF instability is not generally observed in quantum chemistry of typical PAHs. Nevertheless, recently [24] we have encountered one not-so-large structure from the well-known family of GQDs. This is (9,6)-periacene, or shortly (9,6)PA, with 130 carbon atoms, for which the singlet instability, i.e. the presence of a negative eigenvalue of the singlet HF Hessian, was spotted [24]. In accordance with the Cizek-Paldus theory [22] it implies that in (9,6)PA there exists, along with the normal symmetry-preserving solution, the symmetry-breaking HF solution too. Certainly, there also exist many other periacenic GODs and like systems with such peculiarities.

For instance, consider the large triply-triangulenic GQD with 426 carbon atoms suggested in [25] for possible spintronic devices. This GQD was termed in [25] as "Kekulean logic gate structure" (KLGS). It had been examined previously in [26], and now, seeking for large electron- instable π-structures, we return to this KLGS, and indeed the π-electron singlet HF instability turns out to take a place in KLGS as well. Thus, these two GQDs, (9,6)PA and KLGS (Fig. 3), will serve us as relevant examples by which possibilities of the developed BT-SCF algorithm can be investigated.

The same, as in [27] and other works, π-electron semiempirical parameters are employed in all our RHF calculations here. Typically, BT-SCF iterations were performed until achieving the RHF gradient matrix norm of 10^{-10} atomic unit (au). Below the iterative SCF processes are suitably characterized by $\Delta E_{RHF} = E_{CIS} - E_0$, i.e., the difference between the current CIS energy, Eq. (8), and the intial energy (10).

Some words about the alternant symmetry which is a specific π-electron feature of most PAHs. From this symmetry the remarkble Coulson-Rushbrooke-Pople theorem follows for neutral π-systems of conjugated hydrocarbons that have no odd-membered cycles ("alternant" PAHs etc.). The theorem states that within RHF all π-electron net charges are zero, and this is true for any correct π-model. In case of singlet-instable π-systems, final RHF solutions can violate this theorem, and such anomal solutions are typically referred to as "charge density wave" (CDW) solutions. In order to prevent one from obtaining CDW, a special iterative projection method can serve as a simplest remedy that is

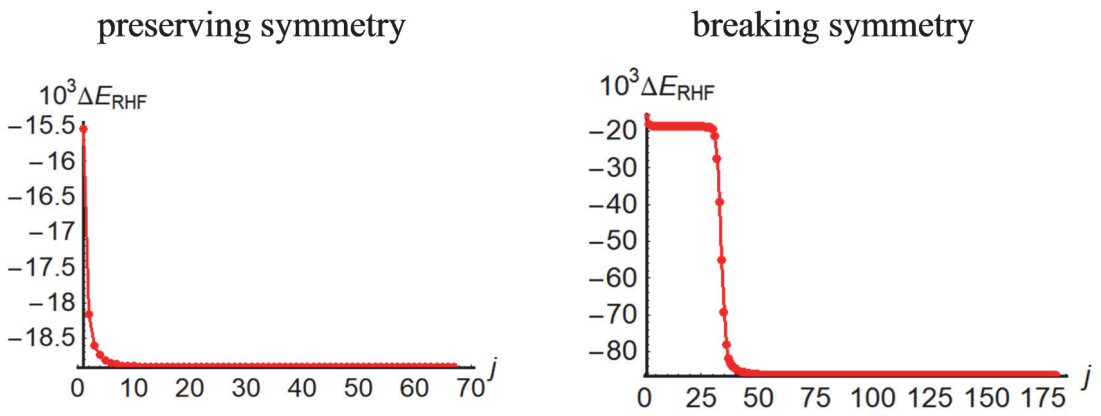

Fig. 2. SCF convergency of symmetry-preserving and symmetry-breaking (CDW) RHF solutions for KLGS.

given below. We make use the certain projection operation in a following manner: at the end of each SCF iteration step the additional correction is made in order to improve the reconstructed matrix P from Eq. (11):

$$P \to (I + P - JPJ)/2. \qquad (12)$$

Here J is the Ruedenberg diagonal matrix [28] in the AO representation. The matrix has nonzero elements consisting of 1 for starred π-centers and −1 for unstarred ones (in Coulson's terms for subdivision of atoms in alternant structures). If ignoring transformation (12), we may arrive to CDW RHF solutions due to rounding errors, provided, of course that RHF instability occurs.

The results obtained for the two basic GQDs are presented in Fig. 1 and 2. We first look at Fig. 1, the left plot, which gives the course of SCF convergence for (9,6)PA in case of the symmetry-preserving solution. As expected, it is seen a systematic energy decrease. In this case the convergence rate is good, and the RHF self-consistency is reached in less than 20 iterations. Another case is the alternant-symmetry breaking solution (the right plot in Fig. 1). In the first 40 iterations, the convergence is markedly slow while a monotonicity in decrease of energy remains as it should be for BT algorithms. Then the almost linear part of the convergence curve is ended and the curve makes a sharp decline to a lower energy solution. The causes for such a behavior are quite understandable. Really, we start from the H?ckel alternant-symmetry solution, and at first the initial alternant symmetry somehow tries to provide a correct solution, so a good symmetry-preserving RHF solution is begining to emerge

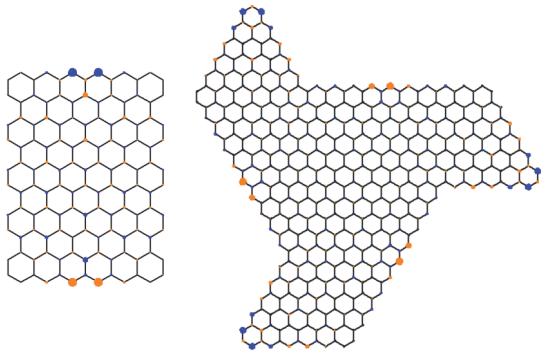

Fig. 3. Atomic net-charge distributions in symmetry-breaking RHF solutions for (9,6)PA and KLGS (positive charges in orange and negative ones in blue).

(when iteration number becomes equal to j *cong* 40). However, rounding errors open possibilities for lowering energy further, and consequently the lower-energy broken alternant-symmetry solution inevitably appears. This picture can be detailed by computing the lowest eigenvalue, $\lambda^{s=0}_{min}$, of the singlet HF-Hessian. In (9,6)PA the RHF solution with a regular symmetry gives $\lambda^{s=0}_{min} = -0.347$ eV [24]. Now performing BT-RHF algorithm (with removing constraint (12)) we will compute $\lambda^{s=0}_{min}$ after each 20th iteration step. The obtained $\lambda^{s=0}_{min}$ set is {−0.746/0, −0.347/20, −0.345/40, 0.230/60, 0.230/80} where denominators are respective iteration numbers (step numbers). In fact, after the 50th iteration the RHF instability is eliminated and we arrive to the RHF stable but broken symmetry solution. The results for KLGS, which are qualitatively the same, are presented in Fig. 2. In this case, we have a higher negative

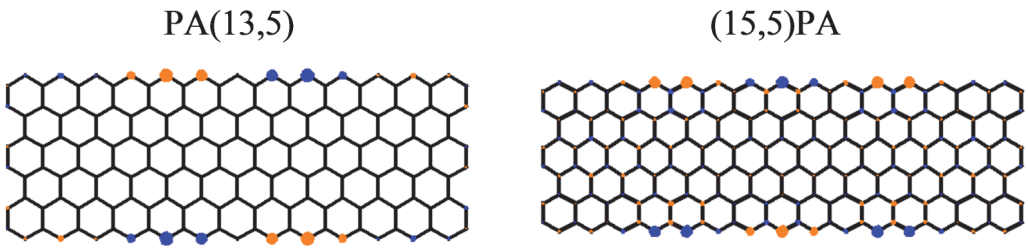

Fig. 4. Atomic net-charge distributions in symmetry-breaking RHF solutions for (13,5)PA and (15,5)PA (positive charges in orange and negative ones in blue).

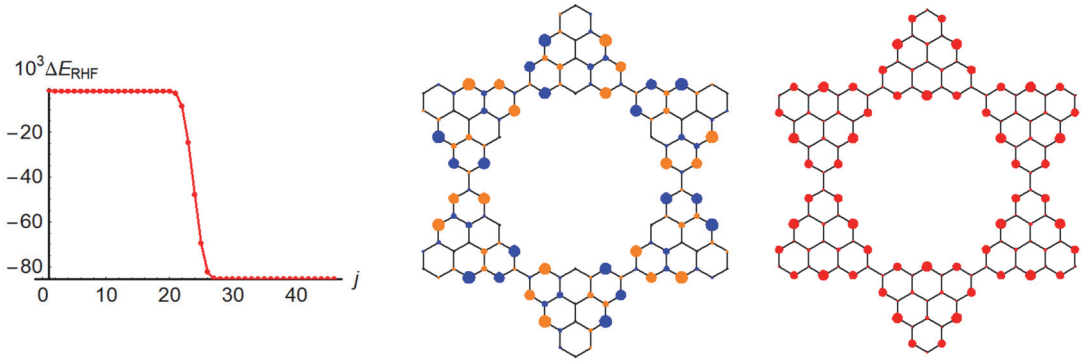

Fig. 5. The π-electron results for TNS. The left panel: SCF convergency of the symmetry-breaking RHF solution. The central panel: the atomic net-charge distribution in the symmetry-breaking RHF solution (positive charges in orange and negative ones in blue). The right panel: the unpaired electron distribution (in red) for the spin-singlet UHF solution.

value $\lambda_{min}^{s=0} = -0.555$ eV for the alternant symmetry solution, and a positive $\lambda_{min}^{s=0} = 0.072$ eV for the final broken symmetry solution.

Notable features are observed in net-charge distributions for the symmetry-breaking solution in these GQDs (Fig. 3). In the case of (9,6)PA the charge distribution is symmetric with respect to x-axis (short axis), and antisymmetric with respect to *y*-axis (long axis). Thus, the total dipole moment vanishes while the average absolute net-charge value (per π-center) is nonzero and equal to 0.042. The KLGS case is rather peculiar because the RHF solution allows breaking the alternant symmetry only. Really, as one can see from Fig. 3 (the left pannel), the net-charge distribution is accurate as satisfying the correct C_{3h} symmetry requirements, and at the same time the average absolute net-charge value is non-null and equal to 0.039. In both cases the dipole moment is obviously absent.

5. Additional examples

We will provide additional illustrations to show other patterns of symmetry-breaking solutions in GQDs. These GQDs are periacene-based systems (13,5)PA and PA(15,5) in Fig. 4, and the unusual triangulenic nanostar (TNS) synthesized in [29] (see below Fig. 5).

For (13,5)PA and PA(15,5) we find the symmetry-breaking solutions with the average absolute net-charge values 0.031 and 0.034, respectively. As any periacene, the (13,5)PA molecule initially possesses the normal D_{2h}-symmety Huckel solution. But the RHF net-charge distribution has a lower C_{2h} "antisymmetry" (not C_{1h} as in (9,6)PA), with null dipole moment as it must be for molecules of C_{2h} symmetry. The net-charge distribution in (15,5)PA has the plain C_{2v} symmetry. Therefore, in (15,5)PA the actual dipole moment for the RHF symmetry-breaking solution is nonzero and equal to 2.26 au.

As the last issue of this section, we will discuss the results for the above-mentioned noval nanostructure TNS (Fig. 5) having 132 carbon atoms. The system also supports two types of RHF solutions, with alternant symmetry and without it. This is in conformity with the stability analysis which gives a large (in modulus) value $\lambda_{min}^{s=0} = -0.722$ eV for TNS. The corresponding course of SCF convergence to the symmetry-breaking solution is displayed in the left panel of Fig. 5. The central panel of the latter shows the charge

net distribution in the obtained solution. It gives the large average absolute net-charge index 0.071 (more twice larger than in the above periacenes).

One peculiarity of TNS should be treated in detail. Indeed, TNS is related to the special class of singular graph structures. They by definition have zero eigenvalues in the associated graph spectra, and thereby in the Hukel orbital spectrum as well (see [30, 31] and references therein). In the case of TNS the graph spectra have 12 zero values (!), but the number of starrred and unstarred carbon atoms (in Coulson's terms) are equal. Then, in TNS the correct ground π-electron state is the singlet state as a consequence of the well-known Lieb-Ovchinnikov rule [32, 33]. Clearly, the TNS H?ckel ground state is the open-shell singlet state with a very high polyradical character. Turn the attention to the fact that in this case (as in case of many other singular graph structures) the RHF approximation destroys the artificial orbital degeneracy inherent in the Huckel description. In fact, by applying the symmetrized Huckel matrix P_{Huck} as a start (with all zero-energy Huckel MOs included with the equal weight 1/2) and employing the BT algorithm we easily obtain the non-degenerate (but unstable) singlet RHF solution discussed above.

Now, we consider the unrestricted Hartree-Fock (UHF) "singlet" solution in TNS. Namely, we will obtain the spin-polarized HF singlet state which is possible only under the so-called triplet instability condition [7, 22]. Note that most periacenes turn out to be triplet instable as well, but the TNS π-system is the particularly interesting example in the context of polyradical π-structure theories. Let us first look at the minimal eigenvalue $\lambda^{s=1}_{\mathrm{min}}$ of the triplet stability matrix. Such $\lambda^{s=1}_{\mathrm{min}}$ predicts the existence of spin-polarized singlet states if $\lambda^{s=1}_{\mathrm{min}} < 0$. For TNS we have $\lambda^{s=1}_{\mathrm{min}} = -3.69$ eV that can be compared with $\lambda^{s=1}_{\mathrm{min}} = -4.29$ eV in (9,6)PA (see Table 11.1 in [24]). Thus, there exists the singlet UHF solution in TNS, and for achieving it we will apply the appropriate BT algorithm (see Appendix for details). The discussion of the TNS properties within UHF is conveniently included in the next section.

6. About peculiarities of symmetry-breaking solutions

Now, we briefly consider possible chemical consequences of symmetry-breaking solutions, using TNS as the example. Notice that in solid-state physics, lowering symmetry is the observable phenomenon having, however, own interpretational questions [34]. In molecular quantum mechanics the situation is also not fully clear, and much depends on the quantum chemistry context (including or not including molecular geometry relaxation etc). Recall that in typical setting of ?- electron problem we fix equilibrium molecular geometry, and thereby molecular Hamiltonian symmetry. Thus any symmetry deviation in resulting RHF solutions should be treated as spurious. Likewize, possible nontrivial UHF solutions do violate spin symmetry, and strictly speaking they are not correct too. However, we can look pragmatically and try to understand which are the artificial HF features that somehow reflect genuine properties of such unstable π-systems.

Particularly, in the UHF description of singlet states we obtain an artificial spin density matrix $Q = \rho_\alpha - \rho_\beta$ giving the so-called spin-density wave (SDW), while Q should be zero in any correctly defined singlet state (McWeeny's theorem). At the same time, in all our examples here the UHF spinless (charge) density matrix $D = \rho_\alpha + \rho_\beta$ is rather good (if ignoring nonzero net charges) and informative because D permits to shed light on an intrinsic radical nature of ground open-shell singlet states. It can be done by invoking the effective unpaired electron (EUE) theory in spirit of Yamaguchi, Head-Gordon and others (see review [35]). Actually, in this theory the key quantity, EUE density matrix D_U from [36] , is a reasonable counterpart of Q for singlet states (see argumentation in [26], Appendix C).

In practice we apply the hole-particle EUE index N_U (N_{eff} in terms of [35]) and corresponding EUE atomic distribution (Eq. (6.39) and (6.41) in loc. cit.). For comparative purposes we will use, as a more suitable index, the specific index $\overline{N}_U = N_U/N$ (with N being the number of carbon atoms), that is the EUE measure per atom. In the case of TNS we find $\overline{N}_U = 0.117$ whereas the same index in (9,6)PA is more than twice smaller $\overline{N}_U = 0.051$, and it agrees with a high polyradical character of TNS. The associated EUE atomic distribution is shown in

the right panel of Fig. 5. We observe that due to high molecular symmetry the unpaired electrons are strongly delocalized, but nonetheless they are most preferably localized on peripherical unstarred atoms. These UHF data for TNS can be compared with those of the simplistic QCTB model developed in [26, 37]: $N_U = 0.115$ for TNS, and $N_U = 0.059$ for (9,6)PA. Within QCTB the EUE atomic distributions are rather similar as well. This demonstrates once more that QCTB provides a good description of SDW and the resulting EUE properties in toto, as previously stated in [26].

Less evident is a clear quantum chemical interpretation of CDW solutions. From simple reasoning, we can state that CDW solutions at the RHF level are possible only for systems with very strong electron correlations. This follows from the noteworthy inequality for $\lambda^{s=0}_{\min}$ and $\lambda^{s=1}_{\min}$ given in [7] (Eq. (2.59)) and [16]:

$$\lambda^{s=1}_{\min} \le \lambda^{s=0}_{\min}. \qquad (13)$$

The latter means that CDW solutions occur only under the triplet RHF instability condition: $\lambda^{s=1}_{\min} < 0$. Thus, if CDW occurs then SDW even more takes a place. Specific examples given above show that the negative $\lambda^{s=0}_{\min}$ appears when the negative $\lambda^{s=1}_{\min}$ is sufficiently large in modulus (e.g., see above the quantities $\lambda^{s=1}_{\min} = -3.69$ eV and $\lambda^{s=0}_{\min} = -0.722$ eV for TNS). Returning to Fig. 5 for TNS we observe (ignoring color difference) a resemblance between the net-charge distribution in the CDW solution (the central panel) and the EUE distribution in the SDW solution (right panel). In other words, most charged atoms in CDW are nearly the same as most electron-unpaired atoms in SDW. From this fact one can draw a plausible conclusion that the both distributions in Fig. 5 provide a similar information about most reactive centers in TNS. The reactivity of the given atomic site μ can be directly characterized by, say, a suitable valence index V_μ which is simply computed within the UHF approximation from the Wiberg bond order indexes (see Eqs. (53), (92), and (113) in [27]). The resulting V_μ diagram is displayed in the shorten form on Fig. 6. As shown in this diagram, the most reactive center has the lowest value $V_\mu = 0.802$ for the same center which is most pronounced in the charge and EUE distributions on Fig. 5. Stress that in alternant

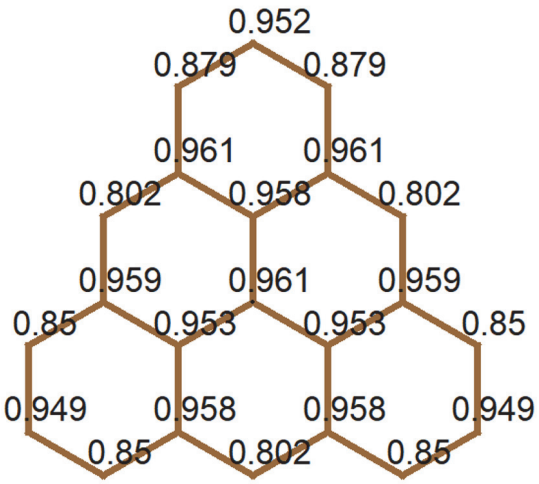

Fig. 6. Atomic valence π-electron diagram for the upper triangulene elementary subunit of TNS.

PAHs all $V_\mu \equiv 1$ at the electron-correlation-free RHF level [27].

Some words are worth saying about the complex-valued HF instability. This well-known instability type was additionally scrutinized in recent interesting works [38, 39]. We have detected a complexed instability in some periacenic structures, but the resultant energy lowering (when passing to the complex-valued MO method) turned out to be too small, and these data are not included in the paper. Seemingly, such small energy effects in the studied GQDs reveal a chemical stability and certain aromaticity [24] of their π-systems. Therefore, these π-systems cannot be abnormal and cannot violate "normal" (aufbau) order of filling real MOs (the interconnection between complexed instability and aufbau principle violation is revealed in [7], section 2.3).

7. Conclusion

The known convergence problem of HF solutions is treated here by the consistent variational use of the Brillouin theorem. It allowed us to elaborate and implement suitable computational schemes that permit obtaining different HF solutions for large graphene-like molecules. In particular, we have managed to obtain the symmetry-preserving and symmetry- breaking HF solutions in periacenic GQDs and in the newest synthesized triangulene-based nanostar structure [29].

Our experience with the given BT algorithm for RHF and UHF π-models demonstrate a good monotonic course of corre-

sponding SCF procedures in the case of symmetry-preserving solutions. A more slower SCF convergence to symmetry-breaking solutions was typical, but the important monotonicy was always observed for total energy as a result of the intrinsically variational nature of the computational schemes used.

As to further perspectives for developing BT based algorithms, we expect that similar approaches can be workable in case of generalized one-electron models such as the known Lowdin's spin-extended Hartree-Fock model and Smeyers's half-projected Hartree-Fock approximation discussed in the literature (e.g., see [40–43]). Preliminary studies show that this is the case, but the full accounts of obtained results are beyond the present paper. In addition, there is a special point concerning a connection of BT algorithms with the related Newton-like optimization scheme named the augmented Hessian (AH) approach given in [44] and many other works (for recent papers see [45–47]).

In the context of the BT algorithm, using AH means that in Eqs. (5,6) one must replace the CIS matrix Π by the normal Hartree-Fock stability matrix Λ implicitly defined in [48] in terms of τ-matrices. Naturally, it would be interesting to compare performace between these two algorithms. Within the AH techhique we have made only few π-electron calculations on small systems, and the SCF converhence in AH turned out to be evidently faster than in BT, but more work should be done to fully clarify the situation. Stress again that the BT technique is consistently variational in energy and appears to be generally more appropriate. Developing this issue is also among our future plans.

Acknowledgement. The paper is dedicated to the remarkable 90th birthday of Prof. Mikhail Markovich Mestechkin, founder of the Ukrainian quantum chemistry school.

Appendix. Solving CIS eigenproblem in AO representation

In the BT algorithm the basic eigenvalue problem, Eqs. (5) and (6), can be specified in the same matrix terms which are known for the HF stability problem [7, 15, 16, 48] and the related matrix computations of CIS excitation energies. A sligthly more broad CIS technique will be given here in order to include its UHF version [18, 19]. Thus, we will deal with the general CIS states built up from the UHF ground-state reference determinant. In this case, instead of P and transition matrix τ, Eq. (4), we need two projectors ρ_α and ρ_β and two transition matrices, τ_α and τ_β, for spin-up and spin-down electrons, respectively. We can return to Eq. (4) by setting

$$\rho_\alpha = \rho_\beta = P, \quad \tau_\alpha = \tau_\beta = \tau/\sqrt{2}. \qquad \text{(A1)}$$

Next, let us introduce a more general than in Eq. (6), superoperator Π acting on τ_α and τ_β, as follows:

$$\hat{\Pi}(\tau_\alpha,\tau_\beta) = (I - \rho_\alpha)[f_\alpha\tau_\alpha - \tau_\alpha f_\alpha + J(\tau_\alpha + \tau_\beta) - K(\tau_\alpha)]\rho_\alpha, \qquad \text{(A2)}$$

with J and K standing for Roothaan's Coulomb and exchange operators respectively. Subsequently, the general CIS eigenproblem can be written in this way:

$$\mathrm{Tr}(f_\alpha\tau_\alpha + f_\beta\tau_\beta) - \lambda c_0 = 0, \qquad \text{(A3)}$$

$$\hat{\Pi}(\tau_\alpha,\tau_\beta) + c_0 f^\alpha_{ph} - \lambda\tau_\alpha = 0, \qquad \text{(A4)}$$

$$\hat{\Pi}(\tau_\beta,\tau_\alpha) + c_0 f^\beta_{ph} - \lambda\tau_\beta = 0, \qquad \text{(A5)}$$

where f_α and f_β are the standard Fock operators ($f_\alpha = h + J(\rho_\alpha + \rho_\beta) - K(\rho_\alpha)$ etc.) for α- and β-shells, and

$$f^\alpha_{ph} = (I - \rho_\alpha)f_\alpha\rho_\alpha, \quad f^\beta_{ph} = (I - \rho_\beta)f_\beta\rho_\beta \qquad \text{(A6)}$$

are the respective UHF gradients. Furthermore, λ has the same meaning as in Eq. (8), but now E is the current UHF energy value:

$$E = \mathrm{Tr}[(h + f_\alpha)\rho_\alpha + (h + f_\beta)\rho_\beta]/2. \qquad \text{(A7)}$$

All the computations can be suitably done by using π-AO basis representation. In particular, π-electron Roothaan's operators J and K (when acting on arbitrary X) are of the form

$$J(X)_{\mu\nu} = \delta_{\mu\nu}\sum_\sigma A_{\sigma\sigma}, \quad K(X)_{\mu\nu} = \gamma_{\mu\nu}A_{\mu\nu}, \qquad \text{(A8)}$$

and $\gamma_{\mu\nu}$ are customary two-center Coulomb integrals for π-AOs. For singlet states, $\hat{\Pi}(\tau_\alpha,\tau_\beta)$ in Eq. (A2) is clearly reduced to $\hat{\Pi}(\tau)$ in Eq. (6) under restrictions (A1). Explicitly,

$$\hat{\Pi}(\tau) = (I - P)[f\tau - \tau f + J(2\tau) - K(\tau)]P. \qquad \text{(A9)}$$

Additionally, in each SCF step we use the Lanczos method [49] for solving the key

eigenproblem, Eqs. (5) and (6), and this usage is also critical for facilitating computations. It is convenient to introduce the total linear operator, Ω, which covers the whole equation system (5) and (6). For simplicity we consider the case of singlet states. By definition, Ω acts on composite "vector" $X = \{c_0, \tau\}$, so that Ω is of the block structure form:

$$\hat{\Omega} = \begin{pmatrix} 0 & \hat{M} \\ \hat{M}^+ & \hat{\Pi} \end{pmatrix}, \qquad \text{(A10)}$$

where alongside $\hat{\Pi}$ we introduce $\hat{M}$ acting on c_0, namely, $\hat{M}(c_0) = \sqrt{2} f_{ph} c_0$. Evidently, Eqs. (5) and (6) are tantamount to the eigenproblem

$$\hat{\Omega}(X) - \lambda X = 0. \qquad \text{(A11)}$$

For completeness let us outline calculation of the lowest energy solution (recall that $\lambda \to 0$ in the BT algorithm). For simplicity consider a Krylov space of size 2 with two basis vectors: a current vector X_0 and corresponding normalized gradient of λ, that is, the matrix $X_1 = [\hat{\Omega}(X_0) - \lambda_0 X_0]/a_0$, where

$$\lambda_0 = \langle X_0 | \hat{\Omega}(X_0) \rangle, \quad a_0 = \| \hat{\Omega}(X_0) - \lambda_0 X_0 \|.$$

In this basis set, Ω is reduced to 2×2 matrix

$$\Omega^{[2]} = \begin{pmatrix} \lambda_0 & a_0 \\ a_0 & \lambda_1 \end{pmatrix} \qquad \text{(A12)}$$

with $\lambda_1 = \langle X_1 | \hat{\Omega}(X_1) \rangle$. Let $\{\beta_0, \beta_1\}$ be a normalized eigenvector of $\Omega^{[2]}$. Then the updated vector $\beta_0 X_0 + \beta_1 X_1$ becomes the new starting vector X_0 in the next Lanczos iteration cycle. Usually, it is sufficient to do 5 Lanczos iterations for yielding good quality solutions to Eq. (8), but for better convergency we recommend to enlarge the Krylov space to size 3 and work with $\Omega^{[3]}$ matrix computed in the same manner. In this case, one additionally constructs the vector $X_2 = [\Omega(X_1) - \lambda_1 X_1 - a_0 X_0]/a_1$, where $1/a_1$ is the normalized factor, and $\lambda_2 = \langle X_2 | \Omega(X_2) \rangle$. Then, by solving eigenproblem for

$$\Omega^{[3]} = \begin{pmatrix} \lambda_0 & a_0 & 0 \\ a_0 & \lambda_1 & a_1 \\ 0 & a_1 & \lambda_2 \end{pmatrix} \qquad \text{(A13)}$$

one produces the updated Lanczos approximation $\beta_0 X_0 + \beta_1 X_1 + \beta_2 X_2$, with $\{\beta_0, \beta_1, \beta_2\}$ being the $\Omega^{[3]}$ lowest energy eigenvector. As seen, no large-scale CIS arrays appear in the above Lanczos iterations, and all the computations are done only on one-electron matrices given in AO basis set.

References

1. P.Tian, L.Tang., K.S.Teng, S.P.Lau, *Mat. Today Chem.*, **10**, 221 (2018).
2. X.-Y.Wang, X.Yao, K.M?llen, *Sci.China Chem.*, **62**, 1099 (2019).
3. A.D.Guclu, P.Potasz, M.Korkusinski, P.Hawrylak, Graphene Quantum Dots, Springer, Berlin (2014).
4. T.Clark, A Handbook of Computational Chemistry: A Practical Guide to Chemical Structure and Energy Calculations, John Wiley, New York (1985).
5. K.N.Kudin, G.E.Scuseria, *ESAIM: Math. Modelling Numer.Anal.*, **41**, 281 (2007).
6. N.D.Wood, M.C.Payne, P.J.Hasnip, *J. Phys.:Condensed Matter.*, **31**, 453001 (2019); S.Lehtola, S.Blockhuys, C.V.Alsenoy, *Molecules*, **25**, 1218 (2020).
7. M.M.Mestechkin, Instability of Hartree-Fock Equations and Stability of Molecules, Naukova Dumka, Kiev (1986) [in Russian].
8. R.Lefebvre, *J.Chim.Phys.*, **54**, 168 (1957).
9. R.Lefebvre, in: Modern Quantum Chemistry, Istanbul Lectures, Pt I Orbitals, ed. by O.Sinanoglu (1965), p.125.
10. S.T.Epstein, The Variational Method in Quantum chemistry, Acad. Press, London (1974).
11. B.Levy, G.Berthier, *Int.J.Quantum.Chem.*, **2**, 307 (1968).
12. F.Grein, T.C.Chang, *Chem Phys.Lett.*, **12**, 44 (1971).
13. M.Godefroid, J.Lievin, J.-Y.Metz, *Int.J. Quantum.Chem.*, **40**, 243 (1991).
14. B.N.Plakhutin, *J.Chem.Phys.*, **153**, 224110 (2020).
15. M.M.Mestechkin, L.S.Gutyra, *Opt.Spektrosk.*, **26**, 159 (1969).
16. M.M.Mestechkin, Density Matrix Method in the Theory of Molecules, Naukova Dumka, Kiev (1977) [in Russian].
17. R.McWeeny, *Queen's Papers Pure and Appl. Math.(Kingston, Ontario)*, **11**, 25 (1968); P.D.Dacre,C.J.Watts, C.R.J.Williams, R.McWeeny, *Mol.Phys.*, **30**, 1203 (1975).
18. A.V.Luzanov, *Theor.Experim.Chem.*, **22**, 489 (1987).
19. A.V.Luzanov, *Funct.Materials*, **24**, 127 (2017).
20. R.McWeeny, *Proc.Roy.Soc.*, **A235**, 496 (1956).
21. R.E.Stanton, *J.Chem.Phys.*, **75**, 5416 (1981).
22. J.Cizek, J.Paldus, *J.Chem.Phys.*, **47**, 3976 (1967).

23. J.Paldus, J.Cizek, *Phys.Rev.*, **A2**, 2268 (1970).
24. A.V.Luzanov, in: Nanooptics, Nanophotonics, Nanostructures, and Their Applications, NANO 2017, Springer Proceedings in Physics, v. 210, ed. by O.Fesenko, L.Yatsenko, Springer, Cham (2018), p.161.
25. Z.Bullard, E.C.Girao, J.R.Owens, *Sci.Rep.*, **5**, 7634 (2015).
26. A.V.Luzanov, F.Plasser, A.Das, H.Lischka, *J. Chem.Phys.*, **146**, 064106 (2017).
27. A.V.Luzanov, O.V.Prezhdo, *Int.J.Quantum. Chem.*, **102**, 582 (2005).
28. K.Ruedenberg, C.W.Scherr, *J.Chem.Phys.*, **21**, 1565 (1953).
29. J.Hieulle, S.Castro, N.Friedrich et al., *Angew. Chem.Int.Ed.*, **60**, 25224 (2021).
30. I.Sciriha, *Electron.J.Linear Algebra*, **16**, 451 (2007).
31. A.V.Luzanov, *Funct.Mater.*, **27**, 800 (2020).
32. A.A.Ovchinnikov, *Theor.Chim.Acta*, **47**, 297 (1978).
33. E.Lieb, *Phys.Rev.Lett.*, **62**, 1201 (1989).
34. X.Zhu, J.Guo, J.Zhang, E.W.Plummer, *Adv. Phys.:X*, **2**, 622 (2017).
35. A.V.Luzanov, in Practical Aspects of Computational Chemistry IV, ed. by J.Leszczynski, M.K.Shukla, Springer, New York (2016), p.151.
36. M.Head-Gordon, *Chem.Phys.Lett.*, **372**, 508 (2017).
37. A.V.Luzanov, *Funct.Materials*, **21**, 437 (2014).
38. T.Yamada, S.Hirata, *J.Chem.Phys.*, **143**, 114112 (2015).
39. W.Small, E.J.Sundstrom, M.Head-Gordon, *J. Chem.Phys.*, **142**, 024104 (2015).
40. M.M.Mestechkin, G.E.Whyman, V.Klimo, J.Tino, Spin-Extended Hartree-Fock Method and Its Applications to Molecules, Naukova Dumka, Kiev (1983) [in Russian].
41. C.A.Jimenez-Hoyos, T.M.Henderson, T.Tsuchimochi, G.E.Scuseria, *J.Chem.Phys.*, **136**, 164109 (2012).
42. Y.G.Smeyers, L.Doreste-Suarez, *Int.J.Quantum.Chem.*, **7**, 678 (1973).
43. V.Botella, O.Castano, P.Fernandez-Serra, Y.G.Smeyers, *Chem.Phys.Lett.*, **219**, 497 (1994).
44. D.R.Yarkony, *Chem.Phys.Lett.*, **77**, 634 (1980).
45. Yu.G.Khait, Yu.V.Puzanov, H.-J.Werner, *J. Mol.Struct.(Theochem)*, **398–399**, 101 (1997).
46. D.A.Kreplin, P.J.Knowles, H.-J.Werner, *J. Chem.Phys.*, **152**, 074102 (2020).
47. B.Helmish-Paris, *J.Chem.Phys.*, 154, 164104 (2021).
48. W.H.Adams, *Phys.Rev.*, **127**, 1650 (1962).
49. B.N.Partlett, The Symmetric Eigenvalue Problem, Prentice Hall, New York (1980).